Shipboard Observations from the North American Monsoon Experiment

PAQUITA ZUIDEMA[1], CHRIS FAIRALL[2], DANIEL WOLFE[2]

[1]*Rosenstiel School of Marine and Atmospheric Sciences, University of Miami, Miami, FL*

[2]*NOAA Earth Research Systems Laboratory/Physical Sciences Division, Boulder, CO*

manuscript submitted to the NAME J Climate Special Issue, Dec. 5

Corresponding author address:

Dr. Paquita Zuidema, RSMAS/MPO, 4600 Rickenbacker Cswy, Miami, FL, 33149-1098 (pzuidema@miami.edu)

ABSTRACT

Observations gathered from the R/V Altair, positioned at the mouth of the Gulf of California from July 7 until August 12, 2004, are presented. 3 gulf surges were noted (July 12-14, Aug. 4, and Aug. 10); the first one is the only associated with a tropical cyclone, and is by far the most pronounced. Most of the warming of the oceanic mixed-layer is associated with the July 12-14 surge. Mean meridional winds were weakly southerly at all levels, while the zonal flow was weakly westerly near the surface, and otherwise easterly, strengthening with height. The 200-hPa flow was westerly until approximately July 17, then easterly thereafter. A trimodal distribution is documented in the relative humidity, ceilometer cloud base heights, and stable (temperature) layers, consisting of a shallow boundary layer capped at approximately 500 m, another layer at 1-2.5 km, and a third layer broadly distributed about the melting level thought to reflect outflow from mainland deep convection. The 1-2.5 km layer appears to be advected moisture generated by deep convection elsewhere. The melting-level layer formed the highest cloud fraction and appears to be outflow from deep convection over mainland Mexico. The diurnal cycle in the boundary-layer winds was primarily meridional, with the predominantly northward winds switching to weakly southward between dawn and noon. Above the boundary layer, winds were north-easterly during the nighttime, with the easterly component rising with height as time progressed, while daytime flow was predominantly westerly above the boundary layer and northerly above 1.5 km. The surface fluxes were similar to those from other field programs in tropical suppressed conditions, with an experiment-mean net heat flux of 70 W m^{-2} into the ocean, primarily through solar absorption.

1. Introduction

Monsoons are fundamentally driven by land-sea heating asymmetries. While the North American Monsoon Experiment (NAME) was well instrumented on land, for logistical reasons observations of the coincident conditions at sea were far fewer. From July 7 until August 12, almost all of the sampling done unambiguously over water was provided by the solitary Research Vessel *R/V Altair* . During this time the *Altair* was auspiciously positioned close to the mouth of Gulf, intermediate between Mazatlan and La Paz. The rawindsondes alone were crucial to the atmospheric moisture budgets construed from the NAME sounding network. In their totality, the Altair observations provide a unique and unprecedented view of the vertical structure, both oceanic and atmospheric, of both the mean background state (for this time period), of the changes associated with the southerly air intrusions known as gulf surges, and of the land-sea breeze diurnal cycle. These observations are presented here.

TABLE 1.

2. Data

Observations were gathered from July 7 until July 22 (“leg 1”), and from July 27 until August 12 (“leg 2”). The ship was positioned approximately at 23.5°N, 108°W (about 80 km distance from land). All instruments on the *Altair* and their measurements are listed in Table 1.

Rawindsondes were typically launched 4 per day, increasing to 6 per day during intensive observation periods (IOPs). IOPs were held on July 12-14 (associated with Tropical Depression Blas), July 20-21...In total, 150 soundings were launched. Other measurements of the boundary layer structure were gathered by a continuously-observing wind profiler, a ceilometer, and a flux system (Fairall et al. 1997). Turbulent fluxes are obtained using motion-corrected eddy covariance (Edson et al. 1998), inertial dissipation (Edson et al. 1991; Fairall et al. 1990), and bulk aerodynamic methods (Fairall et al. 1996). Radiative fluxes are obtained using redundant, carefully calibrated pyranometers and pyrgeometers (Fairall et al. 1998). The vertically-pointing wind profiler (Ecklund et al. 1988) provides continuous profiles of wind and turbulence in the lower few km at 60 and 110 m resolution, even in the absence of precipitation and below

cloud base (by virtue of "clear air refractive index Bragg scattering). From the profile of clear-air backscatter intensity, it also gives the boundary layer depth in almost all conditions. Details on motion stabilization and processing of the wind profiler are given in (Fairall et al. 1997). Oceanic temperature and salinity profiles were gathered 4X/daily to 150 m depth by a conductivity-temperature-depth probe. This probe failed near the beginning of leg 2; all other instrumentation functioned normally.

3. Overview

A succinct overview of the conditions sampled by the *Altair* is provided by a time series of the vertically-averaged 1000-700 hPa winds and the accompanying surface level pressure (Fig. 1). While the mean lower-troposphere winds were often weak, they were at times disrupted by enhanced south-easterly winds. This occurred most promimently on July 12-14, when the Tropical Depression Blas passed to the south and southwest of the Gulf of California. Mean lower troposphere winds reached 12 m s^{-1}. On two other occasions, the mean 1000-700 hPa wind exceeded 3 m/s for approximately 12 hours (Aug. 4 18 UTC - Aug. 5, 6 UTC; Aug. 10 12-20 UTC). These events, unassociated with a tropical cyclone, possessed much weaker winds than those of July 12-14. At times, superimposed upon the mean winds, diurnal variations are apparent; July 12-14 is the most obvious example. FIG. 1.

a. Atmosphere

Fig. 1 lends itself to a compositing of the *Altair* observations into those documenting the mean background state, and those associated with gulf surges. As shown in Fig 2, the experiment-mean wind and moisture profiles show weakly northward meridional flow at all levels, weakly-eastward zonal flow at near-surface levels, with westward flow aloft, strengthening above 600 hPa. A time series lends further insight (Fig. 3). Upper-level 200 hPa winds during leg 1 were still eastward, possibly reflecting a delayed northward springtime migration of the climatological westerly jet. This transitioned over to the more typical westward winds after July 17 (Fig. 3). The

time series of the meridional winds shows low-level northerly winds at times, most notably on July 15-16.

The mean relative humidity profile (Fig. 2c) shows several notable features. One is that the boundary layer is shallow, extending up only to approximately 500 m (also evident in the wind profiler data). The mean near-surface relative humidities do not exceed 73 %[1]. These are presumed to both be features of a generally subsident atmosphere. The other notable feature is the trimodality of the relative humidity distribution. In addition to the boundary layer, broader secondary maxima occur at 1-2.5 km, and at 5-6 km. As shown in a time series of the sounding relative humidity profiles with the winds overlain (Fig. 3), the 1-2.5 km moisture layer is intermittently present. This layer also coincides with the presence of ceilometer-inferred clouds (Fig. 4). At times the clouds at this level may have their bases near the surface (e.g, July 13, late Aug. 5), but more commonly, the moisture and clouds were disconnected from the surface (subsiding with time even, as on July 10-13). On July 19-22 this layer was associated with westward winds, suggesting advection from the Mexican mainland and thus may represent the residue of a deeper land boundary layer. The July 19-21 time period, which wasn't associated with a gulf surge, had the highest water vapor path calculated from the soundings of the entire sample.

The 3rd moisture and cloudiness level was distributed around the melting level (5-6 km) and had the highest cloud fraction of the 3 cloud layers (Fig. 4). The cloudiness was visually ascertained to be liquid-phase altocumulus, rather than ice phase, even though cloud base heights were often ascertained to lie above the mean melting-level of 5.2 km (Fig. 4). This suggests the clouds were often composed of super-cooled liquid. Winds were robustly westward at this level, more so than at the lower levels. The moisture/cloudiness at this level would appear to be melting-level outflow generated from deep convection over the mainland, and thereafter advected to the west (a process also visually ascertained during the experiment).

The vertical distribution of 50-m thick layers with enhanced temperature stability, shown in

[1]Daytime heating of the radiosondes and ship may have impacted the nearest-surface values.

Fig. 5, also shows a trimodality consistent with the distribution of moisture and cloud layers. The 6 km maximum lies slightly above the cloud base height maximum of 5.5 km in Fig. 4.

FIG. 2.

FIG. 3.

b. Ocean

The oceanic mixed layer depth was approximately 20 m (Fig. 6), changing little throughout leg 1. Within the mixed layer, the mean oceanic temperature was near 30 Celsius. The time evolution of the mean 20-m thick upper layer (Fig. 7) properties shows the variability within the mean values. The most pronounced change is a rise of over 1 Celsius in the mixed-layer mean temperature beginning on July 10, reaching a maximum daily-mean temperature of 30.5 on July 12 and decreasing slightly thereafter, though with strong diurnal variations. No discernible salinity change was associated with the strong warming, though after July 13, a slight freshening is evident. Density changes primarily show a responsiveness to the temperature changes. Underneath the mixed layer, a layer of approximately 10 m thickness contained the freshest water sampled, while a near-surface layer of only 1-2 m thickness was also slightly fresher than the water beneath it. Despite the strong solar absorption evident in the diurnal variability, most of the mixed-layer warming during leg 1 can be attributed to advection, rather than local solar absorption.

FIG. 4.

FIG. 5.

FIG. 6.

FIG. 7.

c. Fluxes

The sea surface temperature (SST) was continuously monitored at approximately 5 cm depth by a “sea snake”; its time series is shown in Fig. 8, as well as that of the virtual air temperature. Strong diurnal variations are apparent in the SST[2]. The SST appears to rise during leg 2, approaching a diurnal average of 31 Celsius. The virtual air temperature is typically less than the SST by 1-2 Celsius. Downward spikes are associated with evaporative cooling from precipitation. Evaporation and/or sublimation of precipitation were also frequently observed in

[2]During some quiescent times the ”sea snake” SST thermometer was observed to rest against the boat; this may account for the occasional high temperature spikes, particularly during afternoons with light winds (day 195, 217, 219, and 222)

the wind profiler and ceilometer backscatter intensities. FIG. 8.

A time series of the daily average surface flux component values (Fig. 9) demonstrates that FIG. 9. the solar flux and latent heat fluxes are the dominant terms. High latent heat fluxes are primarily associated with strong wind speed episodes, while variations in radiative fluxes are principally caused by clouds. The impact of clouds on the surface energy budget is best indicated by the cloud forcing, or the difference in the observed mean radiative flux from the clear-sky flux. A time series of the longwave and solar cloud forcing during NAME, with the clear-sky values calculated from a simple model, is shown in Fig. 10. The mean cloud forcing was -70 W m^{-2} for the solar flux, and 10 W m^{-2} for the infrared flux; leg 1 was generally cloudier, while leg 2 contained more variability, with both more clear and more deeply cloudy conditions.

Table 2 shows the mean surface flux component values measured during NAME, as well as those from other recent field experiments held in suppressed tropical conditions. The fluxes sampled during NAME and other field experiments are comparable to each other. The mean net heat input to the ocean during NAME was 70 W m^{-2}, on par with undisturbed periods during TOGA-COARE; without clouds, the net heat input would have been approximately 130 W m^{-2}. TABLE 2. FIG. 10.

4. Diurnal Cycle

The boundary layer diurnal cycle in the winds experienced at the *Altair* measured by both the wind profiler and the flux tower (Fig. 11) contains a consistently eastward zonal component, possibly slightly strengthening in the afternoon, and stronger variability in the meridional component. Winds are usually northward, at approximately 2 m s^{-2} between 3 P.M. LT and midnight, turning into weakly southward between dawn and noon. Fig. 12 shows the diurnal cycle in the wind-profiler-derived winds up to 3 km; note that local time is approximately 7 hours earlier than the given UTC time. Above the boundary layer top ($\sim$ 600 m), the meridional component shifts sharply to southward during the night and into the morning, lasting until about local noon. The zonal component is primarily westward during the night, and includes an interesting rise in the maximum westward wind with height as the night progresses. During the day, the zonal wind

is eastward up to approximately 1.5 km, weakening above. While the nighttime boundary layer top is marked by a change in winds, the daytime boundary layer top is not. The complicated diurnal cycle appears to be dominantly influenced by the mainland Mexico (as opposed to Baja California), with an afternoon inflow to land that is possibly deepened in response to the late-afternoon convection over the Sierra Madre Occidental, and a nighttime land-breeze that also reflects outflow from further north along the Gulf of California. The consistently eastward boundary layer winds, irrespective of time of day, is less easily understood.

The diurnal cycle in the infrared cloud forcing shows almost clear skies in the mid-afternoon, with the largest infrared cloud forcing occurring between midnight and dawn (Fig. 13. This is indicative of higher cloud fractions at this time.

FIG. 11.

FIG. 12.

FIG. 13.

5. Summary and Discussion

This paper has presented some of the basic observations made by the *Altair* during the North American Monsoon Experiment. The results include the documentation of 3 gulf surges at the mouth of the Gulf of California. The first one is the only one associated with a tropical cyclone, and is by far the most pronounced. Decreased surface pressures on July 11 were followed by winds with a northward component reaching 10 m/s and a westward component of 6-8 m/s (Fig. 1). Within the ocean, advection warmed the mixed-layer temperatures by over 1 degree Celsius. The largest surface presicipitation rate noted by the *Altair* during NAME occurred on July 12 12 UTC (6 AM LT), but significant atmospheric sublimation and evaporation of precipitation was also noted, and is arguably an important atmospheric cooling. The wind structure on July 12 was complex, while on July 13 the winds were more strongly northward and associated with increased moisture between 2-6 km. A diurnal cycle is also apparent in the 2 day variation.

The mean winds were weakly northward at all levels, while the zonal flow is weakly eastward within the boundary layer and westward above, strengthening with height. The 200-hPa flow was eastward until approximately July 17, when more climatologically-representative westward flow became established. The ocean mixed layer had an average temperature of 30 degrees Celsius

(Fig. 6 and Fig. 7); although diurnal variations were strong and some locally-driven warming was apparent throughout the course of the experiment (Fig. 8), the primary warming was caused by advection.

The atmospheric relative humidity, cloud vertical distribution, and stable layer distribution clearly shows 3 layers. The boundary layer is shallow, extending up to only 500-600 m, and has a mean relative humidity of only 73 %. Another layer lies between 1-2.5 km, and a 3rd layer is distributed about the melting level. The middle layer is typically not generated locally, but rather, appears to be an advected residual layer, from the south on July 13, and from the east during July 19-21, when it contributed to the highest rawindsonde-inferred water vapor paths measured over the *Altair*. In both cases the moisture was generated by deep convection elsewhere. The melting-level cloudiness formed the highest cloud fraction of the 3 layers. The cloudiness is associated with westward winds, suggesting it is melting-level outflow from deep convection occurring over the Mexican mainland. Interestingly, the cloudiness was often liquid phase, possibly super-cooled, rather than ice phase. This can help explain its persistent presence, as an ice-phase cloud can precipitate away, while the liquid phase can be maintained by infrared radiative cooling. The signature of infrared radiative cooling may also be evident in the vertical distribution of layers with enhanced stability (Fig. 5). More work is required to document and support this hypothesis.

An interesting diurnal cycle was noted. Within the boundary layer, the primary diurnal variability was in the meridional component, with primarily northward winds becoming weakly southward between dawn and noon (Fig. 11). The boundary layer height showed little diurnal variation according to wind profiler measurements. During nighttime the boundary layer top was associated with strong wind shear, with winds switching to southward and the zonal component switching to westward at sunset near the boundary layer top. Thereafter, the vertical location of the westward flow is seen to rise with height as time progresses. During the day, the boundary layer top is not associated with wind shear, and the eastward flow occupies an ever-deepening layer until sunset. The complex diurnal flow is obviously influenced by aspects of the heating of the

mainland Mexico and convection over the Sierra Madre Occidental, but a deeper understanding requires the integration of observations made at other sites.

The surface heat fluxes were dominated by the solar flux and latent heat flux. The experiment-mean net heat flux was 70 W m^{-2}, warming the ocean. This is comparable to that from other recent field experiments held in suppressed tropical conditions. The diurnal cycle in infrared cloud forcing suggests a higher nighttime cloud fraction than daytime.

Acknowledgments. This work was supported by the NOAA Office of Global Programs, in collaboration with the Navy of Mexico. Other scientists participating in the success of the cruise include, from the University of Miami, Javier Zavala-Garay; from Colorado State University, Brenda Dolan, Gustavo Pereira, and Andrea Saunders; the NOAA engineers Scott Abbott and Sergio Pezoa, and the Mexican Navy personnel, in particular Captain, and F. Gonzalez-Belmonte. We thank the many whose dedication made the North American Monsoon Experiment possible.

REFERENCES

Ecklund, W. L., D. A. Carter, and B. B. Balsley, 1988: A UHF wind profiler for the boundary layer: Brief description and initial results. *J. Atmos. Oceanic Tech.*, **5**, 432–441.

Edson, J. B., C. W. Fairall, P. G. Mestayer, and S. E. Larsen, 1991: A study of the inertial-dissipatoin method for computing air-sea fluxes. *J. Geophys. Res.*, **96**, 10,689–10,711.

Edson, J. B., A. A. Hinton, K. E. Prada, J. E. Hare, and C. W. Fairall, 1998: Direct covariance flux estimates from mobile platforms at sea. *J. Atmos. Oceanic Tech.*, **15**, 547–562.

Fairall, C. W., J. E. Hare, and J. B. Snider, 1990: An eight-month sample of marine stratocumulus cloud fraction, albedo, and integrated liquid water. *J. Climate*, **3**, 847–864.

Fairall, C. W., E. F. Bradley, D. P. Rogers, J. B. Edson, and G. S. Young, 1996: Bulk parameterization of air-sea fluxes for TOGA-COARE. *J. Geophys. Res.*, **101**, 3747–3767.

Fairall, C. W., A. B. White, J. B. Edson, and J. E. Hare, 1997: Integrated shipboard measurements of the marine boundary layer. *J. Atmos. Oceanic Technol.*, **14**, 338–359.

Fairall, C. W., P. O. Persson, E. F. Bradley, R. E. Payne, and S. Anderson, 1998: A new look at calibration and use of Eppley precision Infrared radiometers. part I: Theory and application. *J. Atmos. Oceanic Technol.*, **15**, 1229–1242.

Printed December 5, 2005.

Figure Captions

FIG. 1. a) Surface level pressure as measured by the rawindsondes during leg 1 (solid filled circles and smoothed as a line), b) mean 1000-700 hPa rawindsonde meridional and zonal winds from July 7 until July 22. Panels c) and d) are similar to a) and b), but from July 27 until August 12. Note time resolution in all panels varies with the number of rawindsondes per day.

FIG. 2. a) Mean zonal and meridional winds (black and grey lines respectively), b) Standard deviation in the zonal and meridional winds (black and grey lines), and c) mean relative humidity.

FIG. 3. a) Relative humidity time series with vector winds overlain for leg 1, and vertically-integrated water vapor content up to 10 km in lower panel, and b) same as a) but for leg 2.

FIG. 4. a) Time series of ceilometer-derived cloud base heights; note some days are missing. b) Experiment-mean vertical distribution of the ceilometer cloud base heights, expressed as a normalized percentage.

FIG. 5. Frequency of occurrence of stable layers. Stable layers with lapse rates exceeding -5, -4 and -3 K km^{-1} over a 50 m distance are indicated, respectively, by a dotted, solid, and dashed line.

FIG. 6. a) Mean oceanic temperature, b) salinity, and c) density profiles from leg 1.

FIG. 7. Upper oceanic 20 m layer a) temperature, b) salinity, and c) density measurements (solid filled circles and a smoothed line)

FIG. 8. Sea surface temperature measured at approximately 5 cm depth with a “sea snake” (blue line) and the virtual air temperature measured at the flux tower (green line).

FIG. 9. Time series of daily-average surface flux values: net downwelling radiative solar plus infrared (dark blue line); latent (red line); sensible (green line); and net (turquoise line).

FIG. 10. Time series of the surface solar and infrared cloud forcing (dark blue and green lines respectively). Cloud forcing is calculated as the net surface radiative flux - clear-sky surface radiative flux.

FIG. 11. Mean diurnal cycle in the winds measured by the wind profiler at 60 m and 100 m resolution (green and red line, respectively) and at the flux tower (open blue circles), as a function of local time.

FIG. 12. Mean diurnal cycle in wind-profiler-derived winds, as a function of UTC time.

FIG. 13. Infrared cloud forcing at the surface, as a function of local time.

Tables

TABLE 1. *Altair* Instruments and measurements

System	Measurement	Comments
Motion/navigation package	Motion correction for turbulence	(Fairall et al. 1
Sonic anemometer/thermometer	Direct covariance turbulent fluxes	(Fairall et al. 1
Infrared fast H_2O/CO_2 sensor	Direct covariance moisture/CO_2 fluxes	(Fairall et al. 1
Temperature and moisture sensors	Bulk turbulent fluxes	(Fairall et al. 1
Pyranometer/Pyrgeometer	Downward solar and infrared radiative fluxes	redundant; (Fa
25K Vaisala Ceilometer	Cloud-base height	continuous
915-MHz wind profiler	Winds	(Fairall et al. 1
Conductivity-Temperature-Depth probe	Ocean temperature and salinity profiles	
Rawindsondes	Atmosphere temperature, humidity and wind profiles	Vaisala type R
Optical rain gauges	Precipitation rate and accumulation	redundant and

TABLE 2. Surface flux components from recent field experiments, in W m^{-2}

Experiment	net shortwave	net longwave	sensible	latent	net
TOGA-COARE-1	222	-58	-7	-89	65
JASMINE (pre-onset)	260	-49	-5	-115	90
Nauru99	216	-54	-5	-123	33
NAME	241	-57	-5	-108	70

Figures

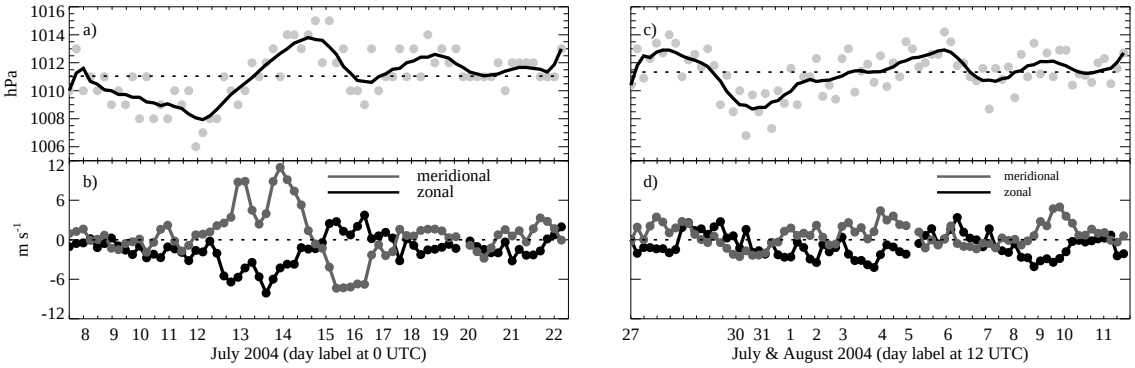

FIG. 1. a) Surface level pressure as measured by the rawindsondes during leg 1 (solid filled circles and smoothed as a line), b) mean 1000-700 hPa rawindsonde meridional and zonal winds from July 7 until July 22. Panels c) and d) are similar to a) and b), but from July 27 until August 12. Note time resolution in all panels varies with the number of rawindsondes per day.

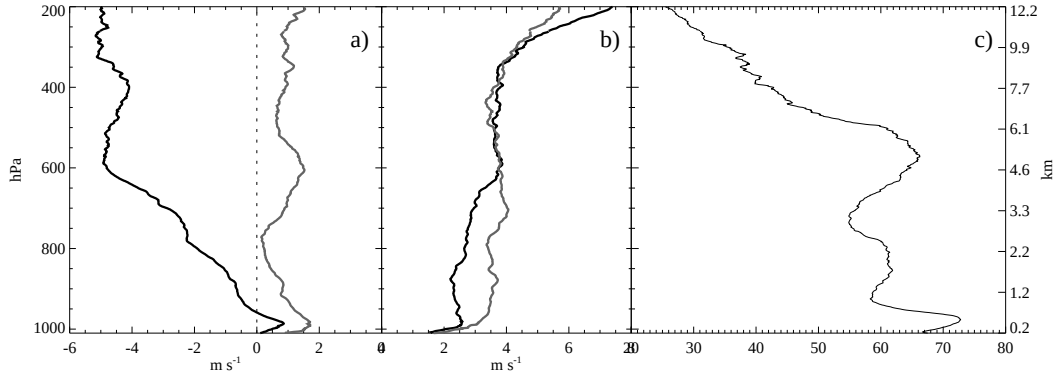

FIG. 2. a) Mean zonal and meridional winds (black and grey lines respectively), b) Standard deviation in the zonal and meridional winds (black and grey lines), and c) mean relative humidity.

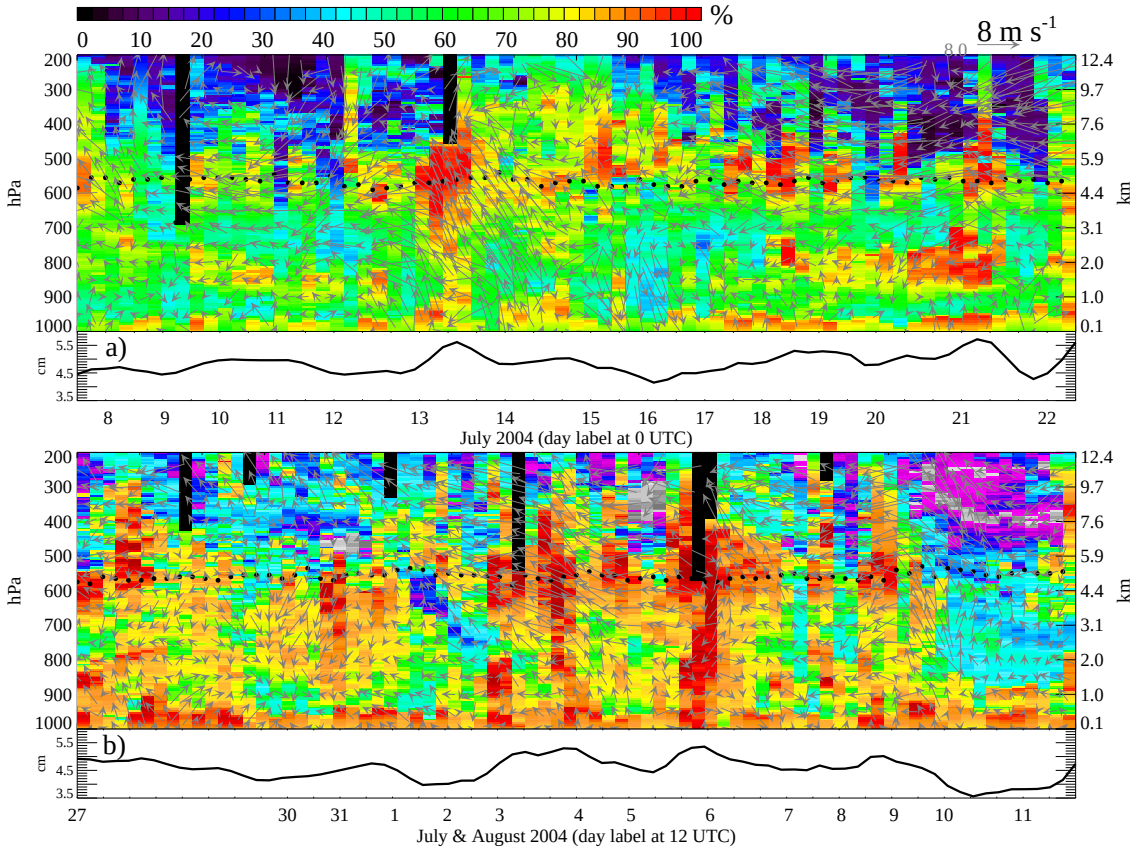

FIG. 3. a) Relative humidity time series with vector winds overlain for leg 1, and vertically-integrated water vapor content up to 10 km in lower panel, and b) same as a) but for leg 2.

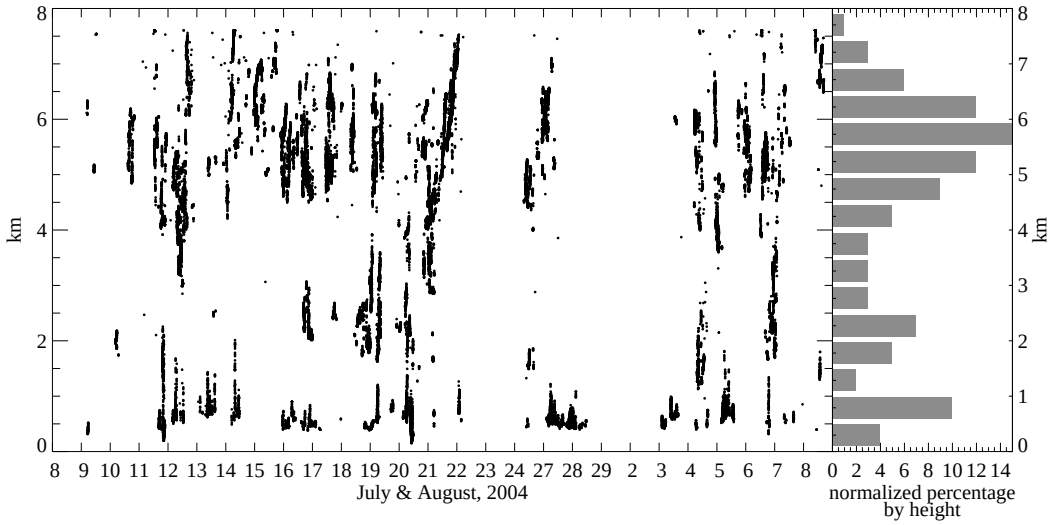

FIG. 4. a) Time series of ceilometer-derived cloud base heights; note some days are missing. b) Experiment-mean vertical distribution of the ceilometer cloud base heights, expressed as a normalized percentage.

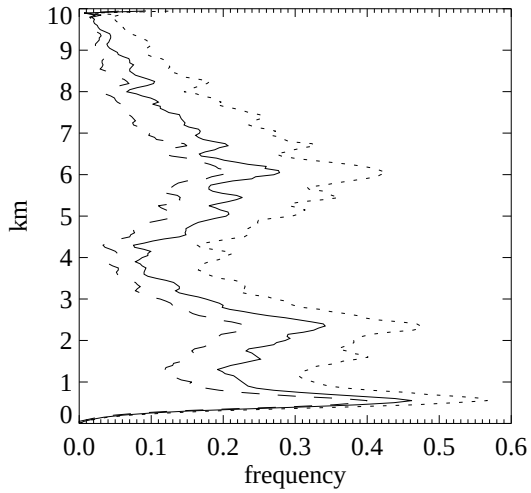

FIG. 5. Frequency of occurrence of stable layers. Stable layers with lapse rates exceeding -5, -4 and -3 K km^{-1} over a 50 m distance are indicated, respectively, by a dotted, solid, and dashed line.

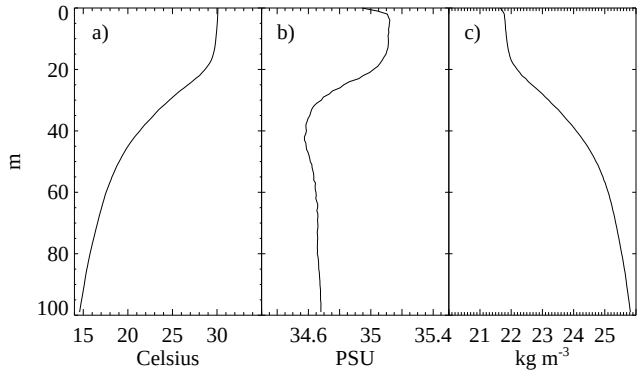

FIG. 6. a) Mean oceanic temperature, b) salinity, and c) density profiles from leg 1.

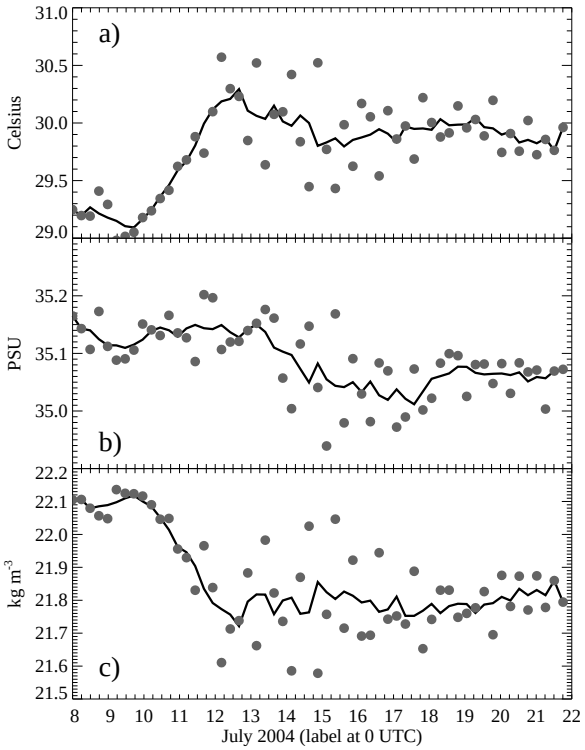

FIG. 7. Upper oceanic 20 m layer a) temperature, b) salinity, and c) density measurements (solid filled circles and a smoothed line)

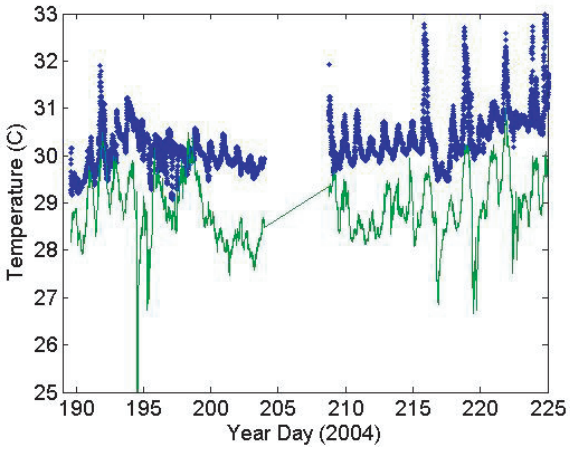

FIG. 8. Sea surface temperature measured at approximately 5 cm depth with a “sea snake” (blue line) and the virtual air temperature measured at the flux tower (green line).

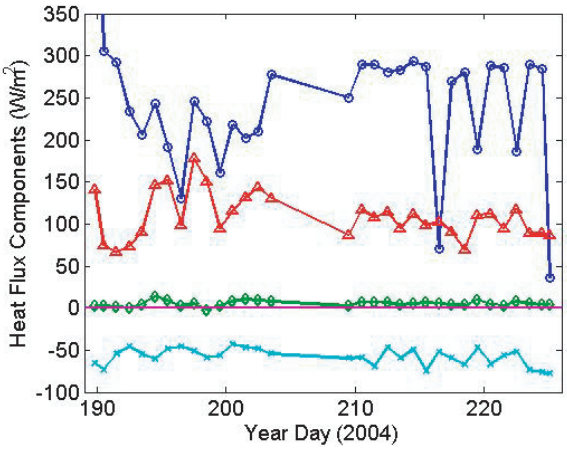

FIG. 9. Time series of daily-average surface flux values: net downwelling radiative solar plus infrared (dark blue line); latent (red line); sensible (green line); and net (turquoise line).

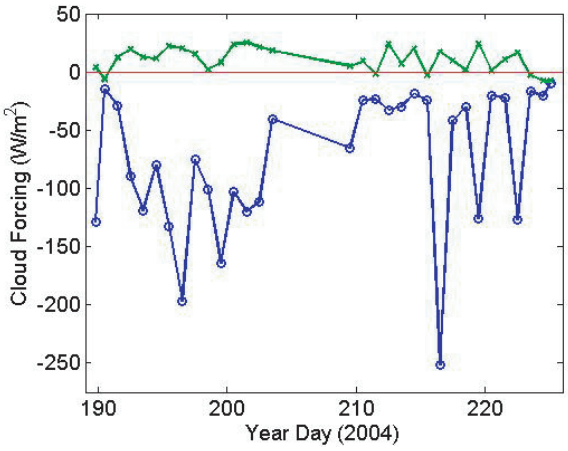

FIG. 10. Time series of the surface solar and infrared cloud forcing (dark blue and green lines respectively). Cloud forcing is calculated as the net surface radiative flux - clear-sky surface radiative flux.

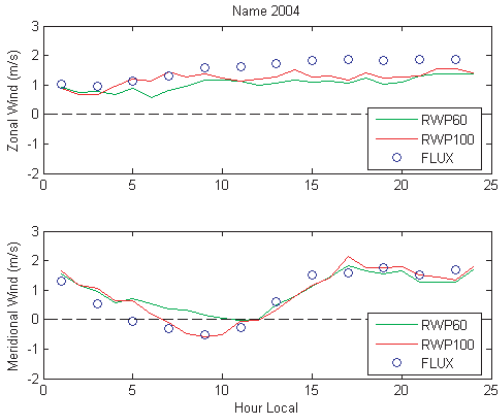

FIG. 11. Mean diurnal cycle in the winds measured by the wind profiler at 60 m and 100 m resolution (green and red line, respectively) and at the flux tower (open blue circles), as a function of local time.

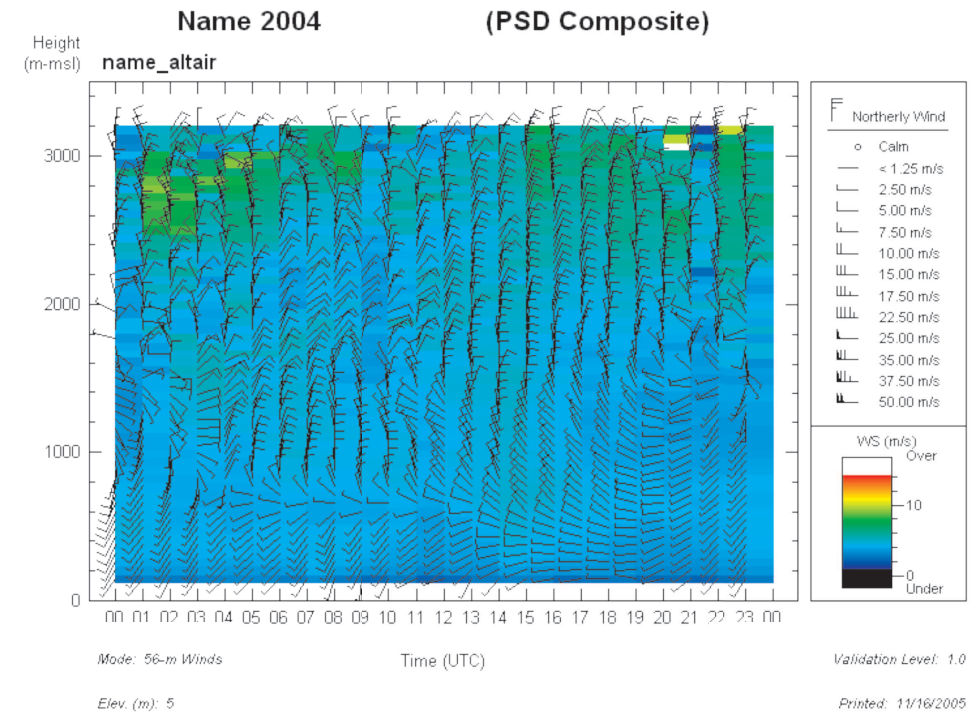

FIG. 12. Mean diurnal cycle in wind-profiler-derived winds, as a function of UTC time.

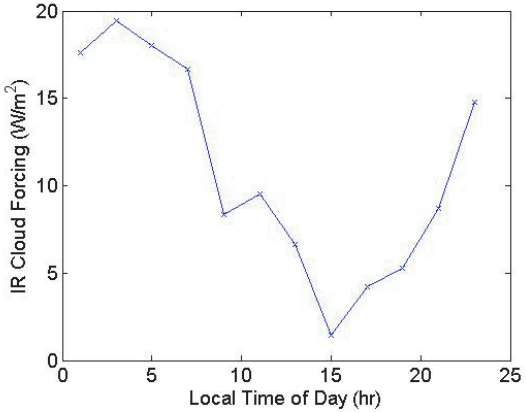

FIG. 13. Infrared cloud forcing at the surface, as a function of local time.